JGR Solid Earth

RESEARCH ARTICLE
10.1029/2026JB034450

Deep Learning Based Upscaling for Predicting Relative Permeabilities Directly From Sub-Volume Images

Jingwei Zhu[1,2], Yuntao Jia[1], Hang Deng[2], Ke Xu[2], Chiyu Xie[1,3,4], and Martin J. Blunt[5]

[1]School of Astronautics, Beihang University, Beijing, China, [2]Department of Energy and Resources Engineering, School of Mechanics and Engineering Science, Peking University, Beijing, China, [3]Ningbo Institute of Technology, Beihang University, Ningbo, China, [4]State Key Laboratory of High-Efficiency Reusable Aerospace Transportation Technology, Beijing, China, [5]Department of Earth Science and Engineering, Imperial College London, London, UK

Key Points:

- We develop a 3DSPPConvUpNet artificial intelligence (AI) model that upscales relative permeability directly from sub-volume digital rock images
- High predictive accuracy across multiscale sandstones (testing MAE < 4%)
- Unseen sandstone cm-scale RPs are reproduced using only 1/16 and 1/12 of their full-rock images, respectively

Supporting Information:

Supporting Information may be found in the online version of this article.

Correspondence to:

C. Xie,
xiechiyu@buaa.edu.cn

Citation:

Zhu, J., Jia, Y., Deng, H., Xu, K., Xie, C., & Blunt, M. J. (2026). Deep learning based upscaling for predicting relative permeabilities directly from sub-volume images. *Journal of Geophysical Research: Solid Earth*, *131*, e2026JB034450. https://doi.org/10.1029/2026JB034450

Received 1 APR 2026
Accepted 20 SEP 2026

Author Contributions:

Conceptualization: Chiyu Xie
Data curation: Martin J. Blunt
Formal analysis: Jingwei Zhu
Funding acquisition: Chiyu Xie
Investigation: Jingwei Zhu
Methodology: Jingwei Zhu
Project administration: Chiyu Xie
Resources: Chiyu Xie, Martin J. Blunt
Software: Jingwei Zhu, Martin J. Blunt
Supervision: Hang Deng, Ke Xu, Chiyu Xie
Validation: Yuntao Jia
Visualization: Yuntao Jia
Writing – original draft: Jingwei Zhu
Writing – review & editing: Hang Deng, Ke Xu, Chiyu Xie, Martin J. Blunt

© 2026 American Geophysical Union. All rights reserved, including rights for text and data mining and training of artificial intelligence technologies or similar technologies.

Abstract Relative permeability (RP) controls multiphase flow in porous media and is therefore central to subsurface applications such as CO_2 sequestration and underground energy storage. Although deep learning has recently enabled RP prediction from digital rocks, direct inference for cm-scale samples is often impractical because high-resolution imaging is costly and has a limited field of view. Here we propose a physics-informed deep learning framework, a three-dimensional (3D) spatial pyramid pooling convolutional upscaling network (3DSPPConvUpNet), that predicts whole-sample RPs from small images together with wettability descriptors. The network embeds scale and geometry information (resolution, sub-volume location, and size proportion) and enforces key physical constraints in the loss function. Across multiscale sandstone data sets, the proposed model achieves high predictive skill (testing MAE $<$ 4%) and reproduces experimental core-scale RPs for two unseen sandstones using only 1/16 and 1/12 of their full-rock structures, respectively. These results demonstrate a practical new route to data-driven RP upscaling when full-core imaging is unavailable.

Plain Language Summary Relative permeabilities describe how easily fluids such as water, oil, CO_2, or hydrogen can move through rocks when more than one fluid phase is present. They are essential inputs for many subsurface engineering problems, but obtaining them for large rock samples is expensive because it requires either laboratory experiments or high-resolution imaging and simulation. We develop a deep learning upscaling method that predicts cm-scale relative permeabilities using only a small portion of the rock image plus basic wettability information. This makes prediction feasible even when scanning an entire large sample is not possible. For two sandstone samples that the model has never seen before, our method matches laboratory measurements well (overall MAE $<$ 5.5%) using only 1/16 and 1/12 of their full-rock structures, respectively.

1. Introduction

Relative permeabilities quantify phase mobilities during multiphase flow in porous media and are key inputs for applications including CO_2 sequestration, geothermal energy, underground hydrogen storage, and hydrocarbon recovery (Eigbe et al., 2023; Huppert & Neufeld, 2014; Murphy et al., 2020; Rezaei et al., 2022). Developments in digital rock imaging (Blunt, 2017) and pore-scale simulation (Zhao et al., 2023) enable RP prediction while preserving pore-scale displacement physics. However, they are costly and rarely feasible for core-scale samples (samples typically a few cm in diameter and length) at high resolution. Moreover, pore-scale estimates do not directly transfer to larger scales because heterogeneity and connectivity effects emerge with increasing support volume (Hussain et al., 2023; Solazzi et al., 2023).

Upscaling methods aim to represent fine-scale flow behavior on coarser grids for core- to field-scale analysis (Liao et al., 2023). Classic approaches (e.g., pressure-averaging and pseudo-function methods) are attractive for their simplicity but can suffer from nonphysical artifacts (e.g., negative upscaled RP) and limited robustness when gravity and capillarity are important (Barker & Thibeau, 1997; Kyte & Berry, 1975). Complementary numerical upscaling workflows based on either saturation distributions (Matthai & Tran, 2023) or lattice Boltzmann (LB) modeling to network modeling (F. Jiang et al., 2022; Xie et al., 2017) can improve fidelity, but remain computationally demanding and typically require full-sample structure information due to the necessity of a representative element volume (REV) (Liu & Wang, 2022; Iyi et al., 2022; Lysyy et al., 2022).

Recent advances in artificial intelligence (AI) and digital rock physics have enabled direct prediction of RPs from wettability descriptors and 3D rock images of various sizes (Cheng et al., 2024; W. Song et al., 2023; Xie, Zhu,

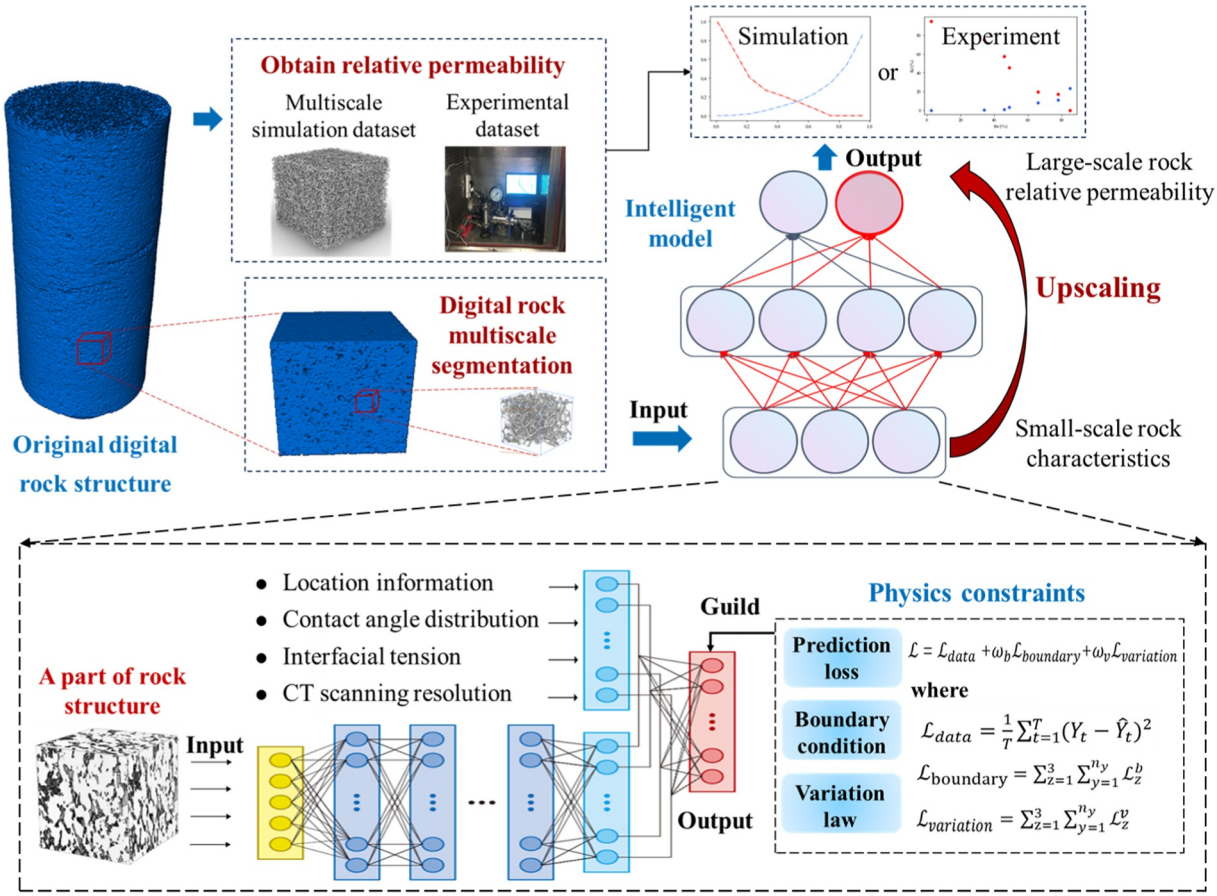

Figure 1. Overview of the upscaling prediction workflow for relative permeability prediction from 3D digital rock images.

Wang, et al., 2023; Xie, Zhu, Yang, et al., 2023). However, applying image-based models to core-scale rocks remains challenging because scanning an entire large sample at pore-scale resolution is expensive and often impossible (Guo et al., 2025; F. Jiang et al., 2023; H. Jiang et al., 2026). As a result, practical upscaling requires learning how to infer whole-sample RP behavior from partial structural information. However, such AI-based approaches tailored for RP upscaling have yet to be established.

Here we develop a physics-informed deep learning upscaling framework, 3DSPPConvUpNet, that predicts core-scale RPs from sub-volume digital rock images. The model (a) embeds scale and geometry information (CT resolution, sub-volume location, and size proportion), (b) incorporates interfacial descriptors (contact angle distribution and interfacial tension), and (c) enforces physical constraints on RP behavior through a physics-informed loss. We validate the method on a multiscale sandstone data set and evaluate its performance against core-scale experiments for two unseen sandstone samples using only 1/16 and 1/12 of the full-rock structure, respectively.

2. Methods

Figure 1 provides an overview of our upscaling prediction of relative permeabilities from pore-scale images, including the AI model design and data set generation. First, we introduce our models based on the proposed physics-based upscaling idea. Next, we describe how the upscaling data sets (including the simulation and experimental data sets) are generated, resulting in 2,815 pairs of data from 10 original digital rock images.

2.1. Physics-Based Upscaling and AI Model Design

According to the universal approximation theorem for neural networks (NNs) (Hornik et al., 1989), the basic form of a deep learning model for upscaling prediction of RP can be written as:

$$Y_j = NN(x_i | W, b), i, j \in N^* \tag{1}$$

where W and b are optimized weights and bias of deep learning model according to data set, respectively. Here, x_i and Y_j denote the ith input parameters and jth output parameters, respectively. For each RP function, every water-saturation point has corresponding oil (or gas) and water relative permeabilities. Therefore, the model output contains three physical quantities: water saturation, oil RP, and water RP:

$$Y = \{Y_j\}_{j=1,2,\ldots,J}, J = 3n, n \in N^* \tag{2}$$

where Y is an output vector representing the RP as a function of water saturation.

Next, the inputs to the NN are determined based on physical knowledge. Many studies have shown that the two key factors affecting the RP are rock structure (Higgs et al., 2023) and wettability (Fan et al., 2020). Rock structure reflects the rock's void-space geometry and provides percolation pathways for two-phase flow (oil/gas and water). Different pathways can produce different flow patterns under otherwise identical conditions, which in turn affects the shape of the RP curves (Bolysbek et al., 2023). Here, we use X-ray CT digital rock images (comprising the multiscale data set $\boldsymbol{S}$) to represent the rock structure:

$$\boldsymbol{S} = \left\{s^{k,r}_{l\times w\times h}\right\}_{k=1,2,\ldots,n}, r, l, w, h \in \left\{N^*, D^+\right\}, n \in N^* \tag{3}$$

where D^+ denotes the set of positive real numbers. Here, $s^{k,r}_{l\times w\times h}$ represents the structure of the kth digital rock image scanned at resolution r, with length, width, and height l, w, and h, respectively. To upscale small-scale rock features to relative permeabilities at the larger (whole-rock-sample) scale, the size of $s^{k,r}_{l\times w\times h}$ is chosen to be at least the representative elementary volume (REV) of the corresponding rock. Wettability affects the capillary forces during two-phase flow (Chen et al., 2023) and therefore influences RP values. Accordingly, we specify the oil–water interfacial tension and the contact-angle distribution for each image to obtain the corresponding RP. We then write:

$$Y^{\text{Whole}} = NN\left(x_S^{\text{Part}}, x_r, x_C, x_{\text{IFT}} \middle| W, b\right), s.t.\ \boldsymbol{S} \tag{4}$$

where x_S^{Part}, x_r, x_C, and x_{IFT} are inputs representing the sub-volume rock structure, CT scanning resolution (reflecting sample size), contact-angle distribution, and interfacial tension, respectively, and Y^{Whole} represents the RP of the whole digital rock.

Furthermore, we introduce two new input features to the upscaling process: the non-dimensional location of the sub-volume within the corresponding whole rock (x_{NLI}) and the spatial length proportion (x_{SLP}). Together, they encode the geometric relationship between the sub-volume and the whole rock sample:

$$Y^{\text{Whole}} = NN\left(x_S^{\text{Part}}, x_r, x_C, x_{\text{IFT}}, x_{\text{NLI}}, x_{\text{SLP}} \middle| W, b\right), s.t.\ \boldsymbol{S} \tag{5}$$

where x_{SLP} can be expressed along the three Cartesian axes as:

$$x^m_{\text{SLP}} = \frac{L^m_{\text{Part}}}{L^m_{\text{Whole}}},\ m = 1, 2, 3 \tag{6}$$

where L^m_{Part} and L^m_{Whole} denote the lengths of the sub-volume and whole rock in the mth direction, respectively.

In words, the model maps a set of physically interpretable inputs to a whole-core RP. The sub-volume image x_S^{Part} captures pore geometry and connectivity that control phase pathways. The resolution x_r indicates the physical scale represented by each voxel and therefore the support volume of the sub-sample. Interfacial properties are represented by the contact-angle distribution x_C and the interfacial tension x_{IFT}, which jointly control capillary forces and displacement patterns. The geometric descriptors x_{NLI} (normalized sub-volume location) and x_{SLP}

(sub-volume-to-whole size fractions along each axis) encode where the sub-sample comes from and how much of the whole it represents. The output Y^{Whole} is the target core-scale RP.

Next, we design the architecture of an intelligent model based on Equation 5. To handle the variable rock sizes in the multiscale data set $\boldsymbol{S}$, the present model is developed form our previous 3DSPPConvNet (Xie, Zhu, Yang, et al., 2023). The 3DSPPConvNet, incorporating 3D spatial pyramid pooling (3DSPP), ConvLSTM, CNN, and FCNN layers, is specifically designed to predict RP from variable-size digital rock images. Here we make three modifications for upscaling prediction. (a) We modify the model inputs and outputs. In this study, the inputs are $(x_S^{\text{Part}}, x_r, x_C, x_{\text{IFT}}, x_{\text{NLI}}, x_{\text{SLP}})$ and the output is Y^{Whole}, whereas in 3DSPPConvNet the inputs are $(x_s, x_r, x_C, x_{\text{IFT}})$ (with x_s denoting the full digital rock structure) and the output is the corresponding RP. (b) In 3DSPPConvNet the rock-structure features are extracted by the 3DSPP module. Here, these features are further weighted by the spatial length proportion before being fed into the next hidden layer (ConvLSTM), which helps improve the prediction accuracy (see Figure S1 in Supporting Information S1):

$$F_{\text{weighted}} = F_{\text{original}} \times \prod_{m=1}^{3} x_{\text{SLP}}^{m} \tag{7}$$

where F_{weighted} and F_{original} represent the space-weighted and original 3DSPP-extracted feature vectors, respectively. (c) We embed the additional geometric descriptor x_{NLI} into the deep FCNN together with $(x_r, x_C, x_{\text{IFT}})$ as shown in Figure 1, whereas 3DSPPConvNet uses only $(x_r, x_C, x_{\text{IFT}})$. Because this upscaling model builds on 3DSPPConvNet, we refer to it as 3DSPPConvUpNet.

Training of 3DSPPConvUpNet still relies on the physics-informed loss function proposed by Xie, Zhu, Yang, et al. (2023), which enforces boundary conditions and the variation law of the RP as physical constraints. The loss function is

$$\mathcal{L} = \mathcal{L}_{\text{data}} + \omega_b \mathcal{L}_{\text{boundary}} + \omega_v \mathcal{L}_{\text{variation}} \tag{8}$$

where $\mathcal{L}$ is the total loss of 3DSPPConvUpNet; ω_b and ω_v are physics-informed weights for the boundary-condition and variation-law terms, respectively; and $\mathcal{L}_{\text{data}}$, $\mathcal{L}_{\text{boundary}}$, and $\mathcal{L}_{\text{variation}}$ denote the data, boundary, and variation losses, respectively (Xie, Zhu, Yang, et al., 2023).

For model comparison, we also train (a) 3DSPPConvUpNet using only $\mathcal{L}_{\text{data}}$ and (b) a 3DSPP support vector regression model for upscaling (3DSPP-SVRUp). In the following sections, we refer to 3DSPPConvUpNet with and without physical constraints as 3DSPPConvUpNetPhy and 3DSPPConvUpNet, respectively. The detailed architectures and hyperparameter settings of all models are provided in Figure S2 in Supporting Information S1. We use a grid-search method (H. Song et al., 2022) to optimize hyperparameters based on three statistical metrics (R^2, MAE, RMSE) suitable for nonlinear algorithms:

$$R^2 = 1 - \frac{\sum_{t=1}^{T} \left(\hat{Y}_t - Y_t\right)^2}{\sum_{t=1}^{T} \left(\hat{Y}_t - \overline{Y}\right)^2} \tag{9}$$

$$\text{MAE} = \frac{1}{T} \sum_{t=1}^{T} \left| \left(\hat{Y}_t - Y_t\right) \right| \tag{10}$$

$$\text{RMSE} = \sqrt{\frac{1}{T} \sum_{t=1}^{T} \left(\hat{Y}_t - Y_t\right)^2} \tag{11}$$

where T is the total number of relative permeabilities in the data set, and $\hat{Y}_t$ and $\overline{Y}$ denote the predicted and mean values of Y_t, respectively. Finally, to quantify the prediction uncertainty arising from different sub-volume images, all predicted upscaled RP are mapped onto a common water-saturation grid. The pointwise ensemble uncertainty is then characterized by the sample mean ± one standard deviation.

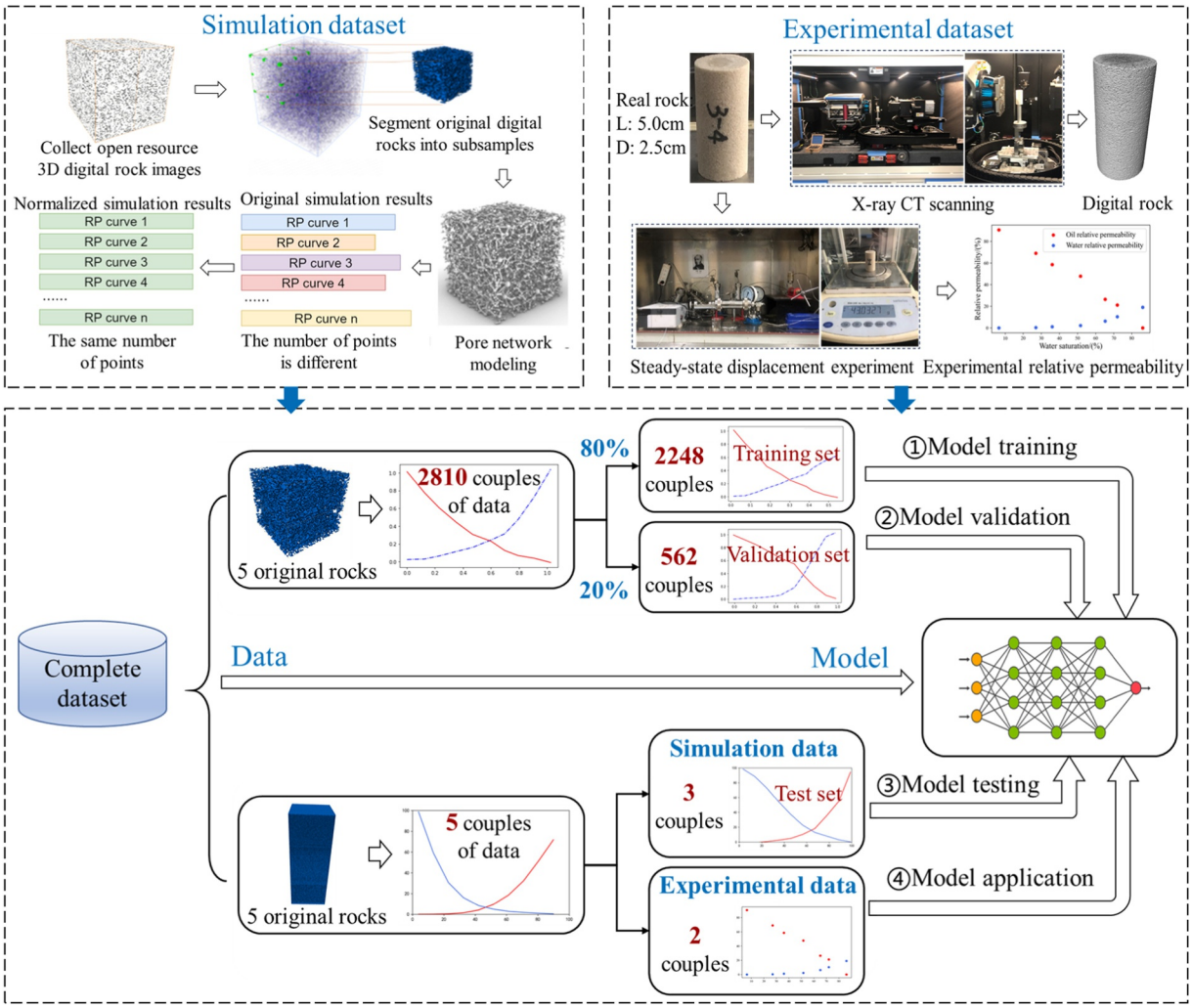

Figure 2. Schematic showing the generation of the complete upscaling data set.

2.2. Data Set Generation

As shown in Figure 2, we construct a complete upscaling dataset—including experimental and simulation data—to train and test three intelligent models. The data set is built from seven publicly available 3D sandstone digital rock images (Bandera Brown, Berea, LV60A, Fontainebleau, Bandera Gray, BSG, and BUG; data sources are listed in Table S1 in Supporting Information S1) and three core-scale 3D sandstones (Sandstone A25, Sandstone A34, and Bentheimer from Lin et al., 2019), with CT scanning resolutions ranging from 2.25 to 26.5 μm. Here, the phase labels of all rock images are unified, with 0 for the pore phase and 1 for the solid phase.

To obtain sub-volumes whose structures map to the relative permeabilities of the corresponding whole-rock images, we segment each rock sample into multiple sub-samples (images are sequentially sliced in a 3D raster-scan manner as shown in Figure 2; code available in https://doi.org/10.5281/zenodo.21784206). Most sub-samples are less than 10 mm across (see Table S2 for sub-sample sizes). The numbers of sub-samples for Bandera Brown, Berea, LV60A, Fontainebleau, and Sandstone A34 are 73, 9, 99, 35, and 218, respectively, yielding 2,810 data pairs for model training, validation, and hyperparameter optimization.

Moreover, we use Bandera Gray, BSG, and BUG (each providing one data pair) to further evaluate model generalization by ensuring that these three rocks are strictly excluded from the training and validation sets and appear only in the test set. Finally, the Sandstone A25 and Bentheimer (Lin et al., 2019) (each providing one data

pair) are employed as upscaling application cases for the well-trained intelligent model (with predictions compared against experimental data).

For the simulation data set, we use an improved pore network model (Xie et al., 2017), validated against experimental data, to generate relative permeabilities for seven publicly available digital rock images. In the simulations, the density, viscosity, and resistivity of water were $1,000\ \mathrm{kg/m^3}$, $1\ \mathrm{mPa \cdot s}$, and $1,82,500\ \Omega \cdot \mathrm{m}$, respectively, while those of oil were $960\ \mathrm{kg/m^3}$, $20\ \mathrm{mPa \cdot s}$, and $10^{13}\ \Omega \cdot \mathrm{m}$, respectively. We consider four contact-angle ranges (with contact angles randomly sampled within each range) spanning from strongly water-wet to strongly oil-wet conditions: 0°–45°, 45°–90°, 90°–135°, and 135°–180°. We also use three oil–water interfacial tension values (20, 40, and 60 mN/m) for Bandera Brown, Berea, LV60A, and Fontainebleau. For Bandera Gray, BSG, and BUG, the contact-angle range and interfacial tension are set to 45°–90° and 40 mN/m, respectively. Because the pore network structures differ, the number of simulated saturation points is different. Therefore, we apply a linear post-processing algorithm (proposed and validated by Xie, Zhu, Yang, et al. (2023)) to normalize all simulated results to a fixed number of output points. Specifically, each RP function is resampled to 10 points.

For the experimental data set, Sandstone A25 and Sandstone A34 (the diameter and length of the samples are around 25 and 51 mm, respectively; see Table S3 in Supporting Information S1) were scanned using X-ray CT at resolutions of 26.39 and 26.50 μm, respectively, and post-processed in Avizo 2019.1 to reconstruct the digital rock images. We then performed steady-state displacement experiments to measure relative permeabilities for both samples. The experimental fluids were water (viscosity $1\ \mathrm{mPa \cdot s}$) and dimethyl silicone oil (viscosity $20\ \mathrm{mPa \cdot s}$), with an interfacial tension of 20 mN/m. Further experimental details are provided in Table S4. For the Bentheimer sandstone, the detailed experimental processes and data can be found in Lin et al. (2019).

3. Results and Discussion

3.1. AI Model Performance

Here, we evaluate model performance on the training, validation, and test sets. As shown in Figure 3a, the training and validation losses for both deep learning models (3DSPPConvUpNetPhy and 3DSPPConvUpNet) gradually decrease and then stabilize as the number of epochs increases, indicating successful training. Compared with 3DSPPConvUpNet, 3DSPPConvUpNetPhy generally achieves a lower loss in both training and validation sets, suggesting improved generalization on the validation set.

Figures 3b–3d show scatter plots comparing predicted and simulated results in the validation set for oil RP, water RP, and water saturation. Most points lie close to the dashed line ($y = x$), indicating good agreement between predictions and simulations. Compared with 3DSPPConvUpNet and 3DSPP-SVRUp, 3DSPPConvUpNetPhy has fewer points deviating from the $y = x$ line, indicating better predictive performance.

Quantitatively, we evaluate three models on the validation set using three statistical metrics (R^2, MAE, and RMSE; calculated across all output components), as summarized in Table 1. Excluding 3DSPP-SVRUp, both 3DSPPConvUpNetPhy and 3DSPPConvUpNet achieve strong performance, with R^2 values of 99.7% and 99.6%, respectively. Among the three models, 3DSPPConvUpNetPhy yields the lowest MAE and RMSE (0.80% and 1.21%, respectively), indicating that the physics-informed constraints improve predictive accuracy.

Further, we use the test samples, Bandera Gray, BSG, and BUG sandstones, to evaluate the generalization ability of 3DSPPConvUpNetPhy (Figures 3e–3g). The predicted results for all three digital rock images agree well with the simulated results, indicating strong generalization to unseen sandstones. It should be noted that, the uncertainty ranges for all three rocks are remarkably small with each prediction obtained by upscaling from 1/8 of its original volume (i.e., the uncertainty arises from eight sub-volume images). Among the three cases, Bandera Gray shows the closest agreement. Quantitatively, the MAE and RMSE between predictions and simulations are shown in Figure 3h; all values are below 4.0% and 5.2%, respectively.

In addition, we examine the effects of three hyperparameters on the predictive accuracy of 3DSPPConvUpNetPhy: the learning rate, the number of ConvLSTM layers, and the physics-informed weights (ω_b and ω_v). As shown in Figure 3i, we test six learning rates (10^{-2}; 5×10^{-3}, 10^{-3}; 5×10^{-4}, 10^{-4}; 5×10^{-5}) and find that 5×10^{-4} is optimal, yielding test MAE and RMSE values of 0.80% and 1.22%, respectively. For the number of ConvLSTM layers, we evaluate three choices (1, 2, and 3) (Figure 3j) and find that two layers yields the best

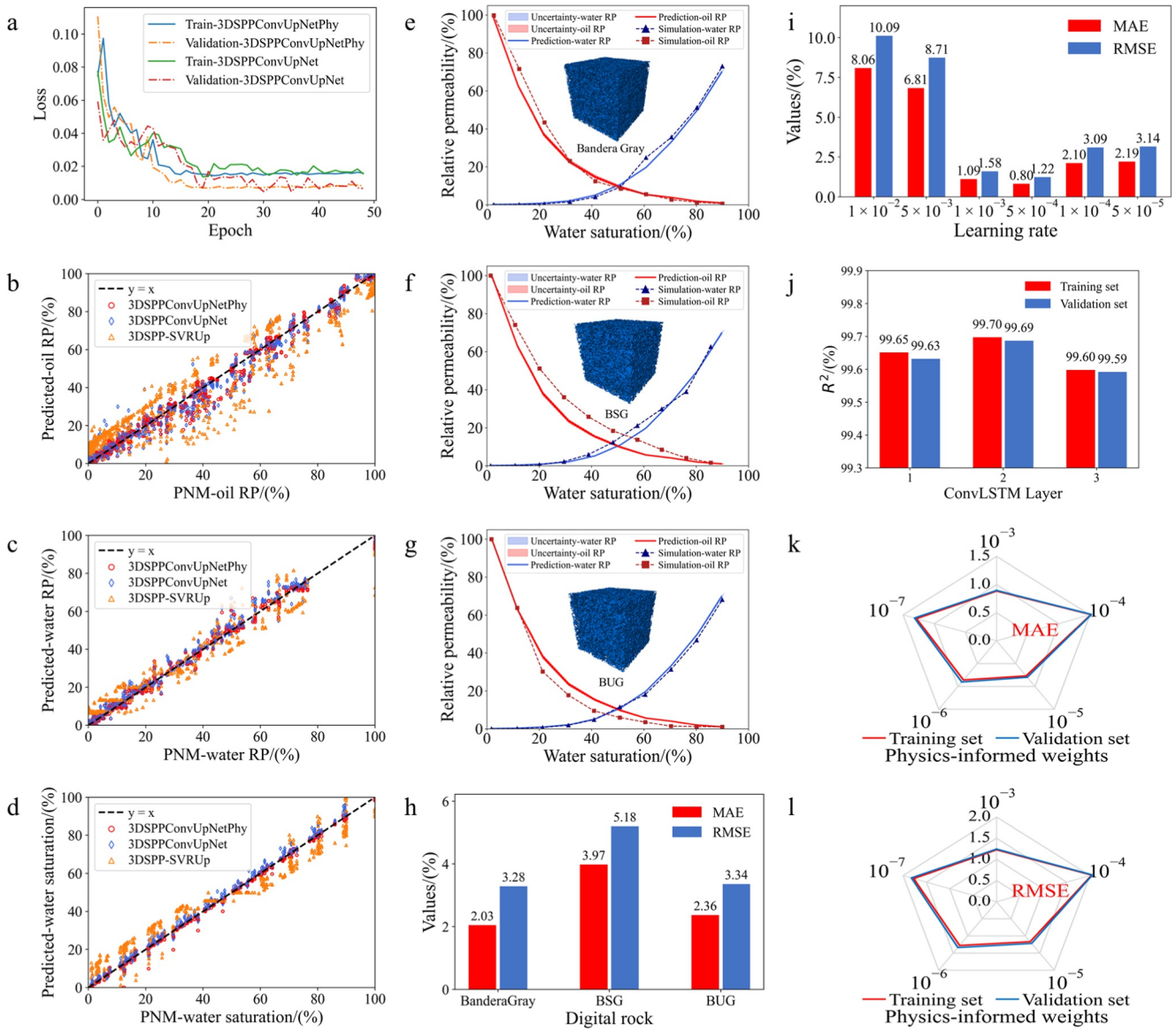

Figure 3. Model performance on the training, validation, and test sets. (a) Training and validation loss curves for 3DSPPConvUpNetPhy and 3DSPPConvUpNet. (b–d) artificial intelligence (AI) predicted versus pore network model (PNM) simulated results for (b) oil relative permeability (RP), (c) water RP, and (d) water saturation. (e–g) AI predicted (with uncertainty ranges) versus PNM simulated relative permeabilities for (e) Bandera Gray, (f) BSG, and (g) BUG in the test set. (h) MAE and RMSE for Bandera Gray, BSG, and BUG. (i) MAE and RMSE under different learning rates in the validation set. (j) R^2 under different numbers of ConvLSTM layers. (k–l) MAE and RMSE under different physics-informed weights.

performance on both the training and validation sets. Figures 3k and 3l show the MAE and RMSE values for five physics-informed weights (10^{-3}, 10^{-4}, 10^{-5}, 10^{-6}, and 10^{-7}). We set ω_b and ω_v to the same value in each case because the boundary and variation constraints are of comparable importance (Xie, Zhu, Yang, et al., 2023). The

Table 1
Statistical Metrics for All Models in the Validation Set

Metrics	3DSPPConvUpNetPhy	3DSPPConvUpNet	3DSPP-SVRUp
R^2/(%)	99.7	99.6	72.7
MAE/(%)	0.80	0.95	6.88
RMSE/(%)	1.21	1.33	7.63

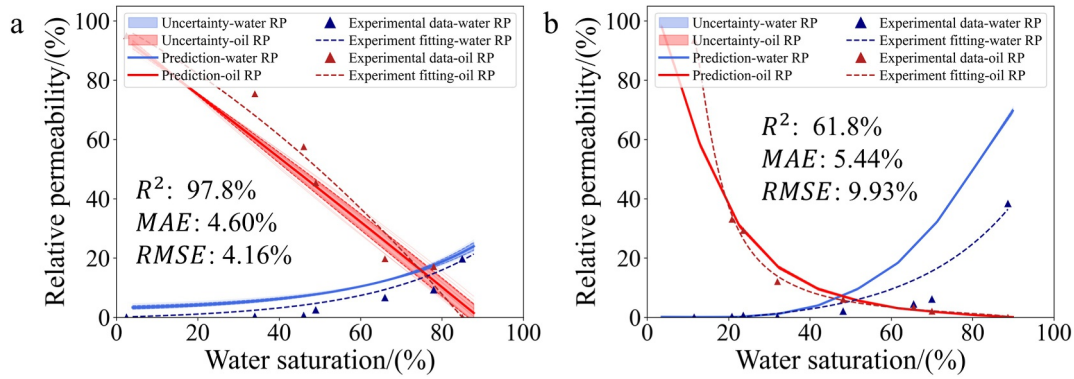

Figure 4. Comparison of experimental data and upscaled relative permeabilities predicted by 3DSPPConvUpNetPhy: (a) Sandstone A25 and (b) Bentheimer.

optimal physics-informed weight is 10^{-5}, which yields the lowest MAE and RMSE on both the training and validation sets.

3.2. Practical Upscaling Applications

Using the well-trained 3DSPPConvUpNetPhy model, we perform practical upscaling predictions for Sandstone A25 and Bentheimer, respectively. As shown in Figure 4, the intelligent upscaling results for both sandstones are compared with the core-scale experimental data (detailed data and fitting equations are available in https://doi.org/10.5281/zenodo.21784206).

For the Sandstone A25 (Figure 4a), all 1/16-sized sub-volume images (335 × 335 × 450 voxels) from the full rock structure (670 × 670 × 1,800 voxels) are fed into 3DSPPConvUpNetPhy (trained under the optimal hyperparameters settings). The predicted relative permeabilities agree well with the experimental data, achieving $R^2 = 97.8\%$ with MAE = 4.60% and RMSE = 4.16%. Moreover, the narrow uncertainty bounds demonstrate the model's robustness to sub-volume variations, further confirming the reliability of the intelligent upscaling model.

We also input larger sub-volume images (1/3 of the full structure; 670 × 670 × 600 voxels) and obtain MAE = 4.41% with limited uncertainty ranges (see Figure S3 in Supporting Information S1). The slightly lower error with more structure indicates that additional structural information may enhance prediction accuracy.

For the Bentheimer (Figure 4b), the complete rock structure (1,160 × 1,100 × 3,000 voxels) is segmented into 12 sub-volumes (580 × 550 × 1,000 voxels), all of which are subsequently input into 3DSPPConvUpNetPhy. The upscaled RP curves show good overall agreement with the experimental results, despite larger deviations in oil RP at low water saturation and in water RP at high water saturation. The overall performance metrics are $R^2 = 61.8\%$, MAE = 5.44%, and RMSE = 9.33%, with remarkably small uncertainty ranges. The reduced prediction accuracy on Bentheimer is primarily attributed to its mixed-wet nature (contact angles ranging from 63° to 97°) and an interfacial tension of 51.5 mN/m (Lin et al., 2019). In contrast, the model training is restricted to water-wet (0°–45° or 45°–90°) or oil-wet (90°–135° or 135°–180°) conditions with discrete interfacial tensions of 20, 40, and 60 mN/m. Besides, it should be noted that 3DSPPConvUpNetPhy used for Bentheimer is trained with a learning rate of 10^{-3}, 2 ConvLSTM layers, and physics-informed weights of 10^{-4}, respectively. This is slightly different from the optimal hyperparameters settings. Therefore, the well-trained 3DSPPConvUpNetPhy model provides a solid foundation for reliable upscaling predictions under the targeted conditions. To generalize it to broader or alternative scenarios, additional relevant data is required for model fine-tuning or further training (e.g., via transfer learning).

4. Conclusions

We develop a physics-informed 3D spatial pyramid pooling convolutional upscaling network (3DSPPConvUpNetPhy) that predicts cm-scale relative permeabilities from sub-volume 3D digital rock images, mostly less than 10 mm across, and wettability descriptors, while encoding scale/geometry information and enforcing

physical constraints. Across a multiscale sandstone data set, the model achieves high predictive skill (MAE $< 4\%$) on the test set. For two unseen cm-scale sandstones (Sandstone A25 and Bentheimer), the predicted relative permeabilities agree well with steady-state experiments using only 1/16 and 1/12 of their full-rock structures, respectively, with MAE $< 5.5\%$ for both cases. This framework provides a practical route for RP upscaling when full-core pore-scale imaging is unavailable and may be extended to other multiphase-flow properties such as capillary pressure.

We recognize that strong heterogeneity and anisotropy in complex geological systems (e.g., fractured rocks, bimodal pore media, or layered samples) can affect the model prediction accuracy. Nevertheless, the present 3DSPPConvUpNetPhy serves as a solid foundation on relatively homogeneous sandstones. Extending the model's applicability to these complex scenarios may be achieved by incorporating additional relevant data through model fine-tuning or further training, which represents an important next step.

Conflict of Interest

The authors declare no conflicts of interest relevant to this study.

Availability Statement

The data files used in this paper are available at Zhu et al. (2026).

Acknowledgments
We acknowledge the financial support from the National Natural Science Foundation of China (Nos. 12302326, 12672322), National Key R&D Program of China (No. 2021YFB1507405), the PetroChina Technical Program (No. 2023DJ84), and the National Science and Technology Major Project (Coal-Major Project, No. 2026ZD1703000). We thank Dr. Linqi Zhu at Imperial College London for his help in providing part of the data.

References

Barker, J. W., & Thibeau, S. (1997). A critical review of the use of pseudorelative permeabilities for upscaling. *SPE Reservoir Engineering*, *12*(2), 138–143. https://doi.org/10.2118/35491-PA

Blunt, M. J. (2017). *Multiphase flow in permeable media: A pore-scale perspective*. Cambridge University Press. https://doi.org/10.1017/9781316145098

Bolysbek, D. A., Kuljabekov, A. B., Uzbekaliyev, K. S., & Assilbekov, B. K. (2023). Effect of rock dissolution on two-phase relative permeabilities: Pore-scale simulations based on experimental data. *Applied Sciences*, *13*(20), 11385. https://doi.org/10.3390/app132011385

Chen, K., Liu, P., Wang, W., Chen, Y., & Bate, B. (2023). Effects of capillary and viscous forces on two-phase fluid displacement in the microfluidic model. *Energy & Fuels*, *37*(22), 17263–17276. https://doi.org/10.1021/acs.energyfuels.3c03170

Cheng, H., Wang, F., Yang, G., Guan, X., Cheng, Z., Li, H., et al. (2024). Prediction of relative permeability from capillary pressure based on the fractal capillary bundle model. *Applied Thermal Engineering*, *239*, 122093. https://doi.org/10.1016/j.applthermaleng.2023.122093

Eigbe, P. A., Ajayi, O. O., Olakoyejo, O. T., Fadipe, O. L., Efe, S., & Adelaja, A. O. (2023). A general review of CO_2 sequestration in underground geological formations and assessment of depleted hydrocarbon reservoirs in the Niger Delta. *Applied Energy*, *350*, 121723. https://doi.org/10.1016/j.apenergy.2023.121723

Fan, M., McClure, J. E., Armstrong, R. T., Shabaninejad, M., Dalton, L. E., Crandall, D., & Chen, C. (2020). Influence of clay wettability alteration on relative permeability. *Geophysical Research Letters*, *47*(18), e2020GL088545. https://doi.org/10.1029/2020GL088545

Guo, Y., Jiang, F., Tsuji, T., Kato, Y., Shimokawara, M., Esteban, L., et al. (2025). Machine learning-based upscaling of rock permeability from pore scale to core scale: Effect of training dataset size and sub-core volumes. *Earth Energy Science*, *2*(1), 100041. https://doi.org/10.1016/j.ees.2025.11.008

Higgs, S., Da Wang, Y., Sun, C., Ennis-King, J., Jackson, S. J., Armstrong, R. T., & Mostaghimi, P. (2023). Comparative analysis of hydrogen, methane and nitrogen relative permeability: Implications for Underground Hydrogen Storage. *Journal of Energy Storage*, *73*, 108827. https://doi.org/10.1016/j.est.2023.108827

Hornik, K., Stinchcombe, M., & White, H. (1989). Multilayer feedforward networks are universal approximators. *Neural Networks*, *2*(5), 359–366. https://doi.org/10.1016/0893-6080(89)90020-8

Huppert, H. E., & Neufeld, J. A. (2014). The fluid mechanics of carbon dioxide sequestration. *Annual Review of Fluid Mechanics*, *46*(1), 255–272. https://doi.org/10.1146/annurev-fluid-011212-140627

Hussain, S. T., Regenauer-Lieb, K., Zhuravljov, A., Hussain, F., & Rahman, S. S. (2023). Asymptotic hydrodynamic homogenization and thermodynamic bounds for upscaling multiphase flow in porous media. *Advances in Geo-Energy Research*, *9*(1), 38–53. https://doi.org/10.46690/ager.2023.07.05

Iyi, D., Balogun, Y., Oyeneyin, B., & Faisal, N. (2022). A numerical study of the effects of temperature and injection velocity on oil-water relative permeability for enhanced oil recovery. *International Journal of Heat and Mass Transfer*, *191*, 122863. https://doi.org/10.1016/j.ijheatmasstransfer.2022.122863

Jiang, F., Guo, Y., Tsuji, T., Kato, Y., Shimokawara, M., Esteban, L., et al. (2023). Upscaling permeability using multiscale X-Ray-CT images with digital rock modeling and deep learning techniques. *Water Resources Research*, *59*(3), e2022WR033267. https://doi.org/10.1029/2022WR033267

Jiang, F., Liu, H., Chen, X., & Tsuji, T. (2022). A coupled LBM-DEM method for simulating the multiphase fluid-solid interaction problem. *Journal of Computational Physics*, *454*, 110963. https://doi.org/10.1016/j.jcp.2022.110963

Jiang, H., Shi, B., Qin, C. Z., Arns, C., & Hassanizadeh, S. M. (2026). Pore-scale rock-typing and upscaling of relative permeability on a laminated sandstone through Minkowski measures. *Water Resources Research*, *62*(1), e2025WR041036. https://doi.org/10.1029/2025WR041036

Kyte, J. R., & Berry, D. W. (1975). New Pseudo functions to control numerical dispersion. *Society of Petroleum Engineers Journal*, *15*(4), 269–276. https://doi.org/10.2118/5105-PA

Liao, Q., Li, G., Tian, S., Song, X., Lei, G., Liu, X., et al. (2023). An efficient analytical approach for steady-state upscaling of relative permeability and capillary pressure. *Energy*, *282*, 128426. https://doi.org/10.1016/j.energy.2023.128426

Lin, Q., Bijeljic, B., Berg, S., Pini, R., Blunt, M. J., & Krevor, S. (2019). Minimal surfaces in porous media: Pore-scale imaging of multiphase flow in an altered-wettability Bentheimer sandstone. *Physical Review E*, *99*(6), 063105. https://doi.org/10.1103/PhysRevE.99.063105

Liu, T., & Wang, M. (2022). Critical REV size of multiphase flow in porous media for upscaling by pore-scale modeling. *Transport in Porous Media*, *144*(1), 111–132. https://doi.org/10.1007/s11242-021-01621-2

Lysyy, M., Føyen, T., Johannesen, E. B., Fernø, M., & Ersland, G. (2022). Hydrogen relative permeability hysteresis in underground storage. *Geophysical Research Letters*, *49*(17), e2022GL100364. https://doi.org/10.1029/2022GL100364

Matthai, S. K., & Tran, L. K. (2023). Numeric determination of relative permeability of heterogeneous porous media with capillary discontinuities. *Advances in Water Resources*, *175*, 104430. https://doi.org/10.1016/j.advwatres.2023.104430

Murphy, Z. W., DiCarlo, D. A., Flemings, P. B., & Daigle, H. (2020). Hydrate is a nonwetting phase in porous media. *Geophysical Research Letters*, *47*(16), e2020GL089289. https://doi.org/10.1029/2020GL089289

Rezaei, A., Hassanpouryouzband, A., Molnar, I., Derikvand, Z., Haszeldine, R. S., & Edlmann, K. (2022). Relative permeability of hydrogen and aqueous brines in sandstones and carbonates at reservoir conditions. *Geophysical Research Letters*, *49*(12), e2022GL099433. https://doi.org/10.1029/2022GL099433

Solazzi, S. G., Jougnot, D., Rubino, J. G., & Holliger, K. (2023). Dynamic relative permeabilities for partially saturated porous media accounting for viscous coupling effects: An analytical solution. *Transport in Porous Media*, *147*(3), 653–677. https://doi.org/10.1007/s11242-023-01920-w

Song, H., Zhu, J., Wei, C., Wang, J., Du, S., & Xie, C. (2022). Data-driven physics-informed interpolation evolution combining historical-predicted knowledge for remaining oil distribution prediction. *Journal of Petroleum Science and Engineering*, *217*, 110795. https://doi.org/10.1016/j.petrol.2022.110795

Song, W., Prodanovic, M., Santos, J. E., Yao, J., Zhang, K., & Yang, Y. (2023). Upscaling of transport properties in complex hydraulic fracture systems. *SPE Journal*, *28*(3), 1026–1044. https://doi.org/10.2118/212849-PA

Xie, C., Raeini, A. Q., Wang, Y., Blunt, M. J., & Wang, M. (2017). An improved pore-network model including viscous coupling effects using direct simulation by the lattice Boltzmann method. *Advances in Water Resources*, *100*, 26–34. https://doi.org/10.1016/j.advwatres.2016.11.017

Xie, C., Zhu, J., Wang, J., Yang, J., & Song, H. (2023). Direct prediction of relative permeability curve from 3D digital rock images based on deep learning approaches. *International Journal of Rock Mechanics and Mining Sciences*, *170*, 105544. https://doi.org/10.1016/j.ijrmms.2023.105544

Xie, C., Zhu, J., Yang, H., Wang, J., Liu, L., & Song, H. (2023). Relative permeability curve prediction from digital rocks with variable sizes using deep learning. *Physics of Fluids*, *35*(9), 096605. https://doi.org/10.1063/5.0167998

Zhao, J., Wang, J., Zhang, G., Zhou, D., Chen, L., Viswanathan, H., & Kang, Q. (2023). Minireview on lattice Boltzmann modeling of gas flow and adsorption in shale porous media: Progress and future direction. *Energy & Fuels*, *37*(3), 1511–1524. https://doi.org/10.1021/acs.energyfuels.2c03298

Zhu, J., Jia, Y., Deng, H., Xu, K., Xie, C., & Blunt, M. (2026). Code and data for deep learning-based upscaling for predicting relative permeabilities directly from sub-volume images [Dataset]. *Zenodo*. https://doi.org/10.5281/zenodo.21784206